A topography-based scaling algorithm for soil hydraulic parameters at hillslope scales: Field testing

Raghavendra B. Jana[1] and Binayak P. Mohanty[1]

Received 27 July 2011; revised 24 November 2011; accepted 5 January 2012; published 18 February 2012.

[1] Soil hydraulic parameters were upscaled from a 30 m resolution to a 1 km resolution using a new aggregation scheme (described in the companion paper) where the scale parameter was based on the topography. When soil hydraulic parameter aggregation or upscaling schemes ignore the effect of topography, their application becomes limited at hillslope scales and beyond, where topography plays a dominant role in soil deposition and formation. Hence the new upscaling algorithm was tested at the hillslope scale (1 km) across two locations: (1) the Little Washita watershed in Oklahoma, and (2) the Walnut Creek watershed in Iowa. The watersheds were divided into pixels of 1 km resolution and the effective soil hydraulic parameters obtained for each pixel. Each pixel/domain was then simulated using the physically based HYDRUS-3-D modeling platform. In order to account for the surface (runoff/on) and subsurface fluxes between pixels, an algorithm to route infiltration-excess runoff onto downstream pixels at daily time steps and to update the soil moisture states of the downstream pixels was applied. Simulated soil moisture states were compared across scales, and the coarse scale values compared against the airborne soil moisture data products obtained during the hydrology experiment field campaign periods (SGP97 and SMEX02) for selected pixels with different topographic complexities, soil distributions, and land cover. Results from these comparisons show good correlations between simulated and observed soil moisture states across time, topographic variations, location, elevation, and land cover. Stream discharge comparisons made at two gauging stations in the Little Washita watershed also provide reasonably good results as to the suitability of the upscaling algorithm used. Based only on the topography of the domain, the new upscaling algorithm was able to provide coarse resolution values for soil hydraulic parameters which effectively captured the variations in soil moisture across the watershed domains.

Citation: Jana, R. B., and B. P. Mohanty (2012), A topography-based scaling algorithm for soil hydraulic parameters at hillslope scales: Field testing, *Water Resour. Res.*, *48*, W02519, doi:10.1029/2011WR011205.

1. Introduction

[2] Topography is one of the key controls of soil moisture variability at large scales [*Mohanty and Mously*, 2000; *Famiglietti et al.*, 1998; *Hawley et al.*, 1983]. Along with the topography, soil physical properties, vegetation, and climate have been shown to be the drivers of soil moisture variation over large scales [*Famiglietti et al.*, 1998; *Yeh and Eltahir*, 1998]. Topographic features generate surface runoff and lateral flows in the vadose zone. It can be argued that the variations in soil moisture are also due to the variations in soil hydraulic parameters, which, in turn, are influenced by the soil formation and deposition patterns [*Kohnke and Franzmeier*, 1995]. It has been shown by *Lag* [1951] and *Tedrow* [1951] that soils having similar morphological and genetic histories, and subjected to similar crop practices, displayed different drainage properties based on the topography and the position of the landscape. Soil layer depths vary from location to location. Generally, valleys have deeper soil profiles than locations at higher elevations where the soil depth is determined by the slope steepness [*Hillel*, 1991]. *Wilson et al.* [2004] reported in a study covering five catchment areas in Australia and New Zealand that the topography and the spatial variation of soil properties and vegetation played equally important roles in the variability of soil moisture patterns. Similar findings were reported by *Western et al.* [2004] who found that the topography played a dominant role in dictating soil moisture patterns as compared to soil hydraulic parameter variability. In an analysis of the Swedish National Forest Soil Inventory data, *Seibert et al.* [2007] found that, at the landscape scale, topography was important in dictating soil formation and deposition, and hence, their properties.

[3] Different hydrological phenomena occur due to different causes at a wide range of scales. Modeling of hydrological processes and phenomena, especially those occurring in the unsaturated zone at various scales, is currently a topic of much interest in the scientific community [*Vereecken et al.*,

[1]Department of Biological and Agricultural Engineering, Texas A&M University, College Station, Texas 77843, USA.

0043-1397/12/2011WR011205

2007; *Wu and Li*, 2006; *Zhu and Mohanty*, 2002a, 2002b, 2002c, 2003, 2004, 2006; *Zhu et al.*, 2004, 2006]. Modeling of contaminant fate and transport from point and some non-point sources through the porous media generally takes place at high (fine) resolutions [e.g., *Engesgaard and Traberg*, 1996]. Climate forecasting and circulation models utilize land surface parametric data at much coarser resolutions [e.g., *Williams et al.*, 1974]. In between these, there are medium resolution models for streamflow generation and water balance computation among recharge, evapotranspiration, soil storage, and seepage fluxes across a catchment or watershed [e.g., *Bloschl and Sivapalan*, 1997]. Land surface input data such as soil hydraulic properties are required for each of the above mentioned models at their representative scales. Often the requisite data are measured at a scale inconsistent with the inherent scale at which these models work. This is due to the fact that measurement of parameter data at all such required and different scales is impractical as that would entail huge outlays of finance, time, and effort. Hence the need for scaling schemes which enable one to convert available measured fine resolution data to effective coarser resolution aggregate values, or vice versa. The Miller similitude theory [*Miller and Miller*, 1956] took the first step toward this goal by representing the dimensions of soil particles and pores in terms of a characteristic length scale.

[4] While the assumption of a flat terrain during scaling of soil hydraulic parameters may be reasonable at smaller scales [*Mohanty and Zhu*, 2007], it is not really justifiable at larger scales such as hillslopes and beyond. Scaling schemes applied to such large domains mandate that the physical controls influencing soil parameter values be incorporated into these schemes. The inclusion of the effect of topography in the upscaling algorithm when considering large extents is a step in this direction. In the accompanying companion paper [*Jana and Mohanty*, 2012] we developed an upscaling algorithm which considered the topographic characteristics of the domain, and tested it with several hypothetical scenarios using numerical experiments. Here we present a study to validate the influence of topographic variations on the effective, upscaled soil hydraulic parameters at hillslope scales using real-world field data from two hydroclimatically different locations—the Little Washita watershed in Oklahoma, and the Walnut Creek watershed in Iowa. The primary objective of the study was to obtain effective upscaled values of soil hydraulic parameters such as the saturated hydraulic conductivity, the saturation and residual soil water contents, and the van Genuchten parameters, at the 1 km × 1 km domain/pixel size (hillslope scale) for entire watersheds while incorporating the influence of the local topography into the scaling algorithm.

2. Methods and Materials

2.1. Study Areas

2.1.1. Little Washita Watershed, OK

[5] The Little Washita (LW) River watershed (Figure 1) in Oklahoma was selected as the first test site for this study. Covering parts of Caddo, Comanche, and Grady counties of

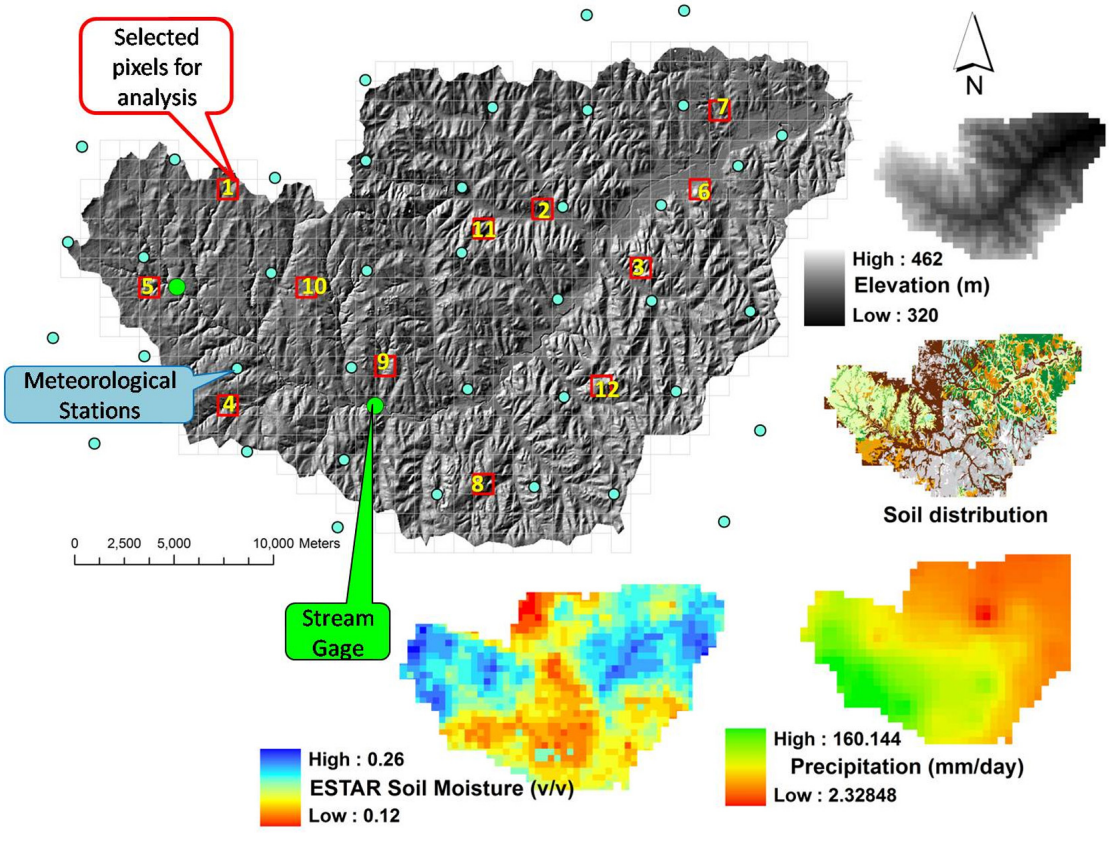

Figure 1. Little Washita watershed study area, location of selected pixels, stream gauges, meteorological stations, and some input layers for modeling.

Oklahoma, the Little Washita River watershed has an area of about 600 square kilometers, situated in the Southern Great Plains region of the United States [*Mohanty et al.*, 2002]. The Little Washita River is a tributary of the Washita River, which drains into the Red River on the Oklahoma-Texas border. Hydrological and meteorological measurements of the watershed have been conducted for decades, providing scientists a long-term data source to study soil and water conservation, water quality, and basin hydrology [*Elliott et al.*, 1993]. Under continuous hydrological observation since 1936, the watershed has a network of sensors spread across its extent to measure rainfall, temperature, relative humidity, and soil radiation. In the 1990s, the United States Department of Agriculture's Agricultural Research Service (USDA-ARS) set up a network of 42 environmental monitoring stations called the ARS Micronet across this watershed. The watershed has also been the focus of several field experiments such as the Washita '92, Washita '94, Southern Great Plains 1997 (SGP97), Soil Moisture Experiments 2003 (SMEX03), and the Cloud and Land Surface Interaction Campaign (CLASIC) 2007.

[6] The LW region has a moderately rolling topography. The maximum elevation of the watershed is about 500 m above mean sea level, with a maximum relief of about 180 m. Rangeland and pastures are the dominant land use, with patches of winter wheat and other crops [*Allen and Naney*, 1991]. Soil textures range from fine sand to silty loam, with few exposed bedrock areas. The climate of the region is classified as subhumid/moist, with a mean annual precipitation of 760 mm and mean annual temperature of 16°C.

2.1.2. Walnut Creek Watershed, IA

[7] The Walnut Creek (WC) watershed (Figure 2) in Iowa was selected as the secondary test site for this study. This watershed is situated to the south of the city of Ames, and covers about 100 square kilometers. This watershed was the focus of the SMEX02 field experiments [*Kustas et al.*, 2003] and continuing research by the USDA-ARS National Soil Tilth Lab.

[8] The WC region has an undulating terrain. Most of the land cover in this watershed is made up of agricultural crops such as corn and soybean [*Doriaswamy et al.*, 2004]. The surface soil in this region is mainly silty clay loam with high organic content [*Das et al.*, 2008]. The region has a humid climate with an average annual rainfall of about 835 mm, May and June being the months of heaviest precipitation. Maximum topographic relief of the watershed is about 60 m.

2.2. Aggregation Methodology

[9] The power average operator, as described by *Yager* [2001] is used in this study to coarsen the soil hydraulic parameter values. This technique, which has been described in detail in the companion paper to this study [*Jana and*

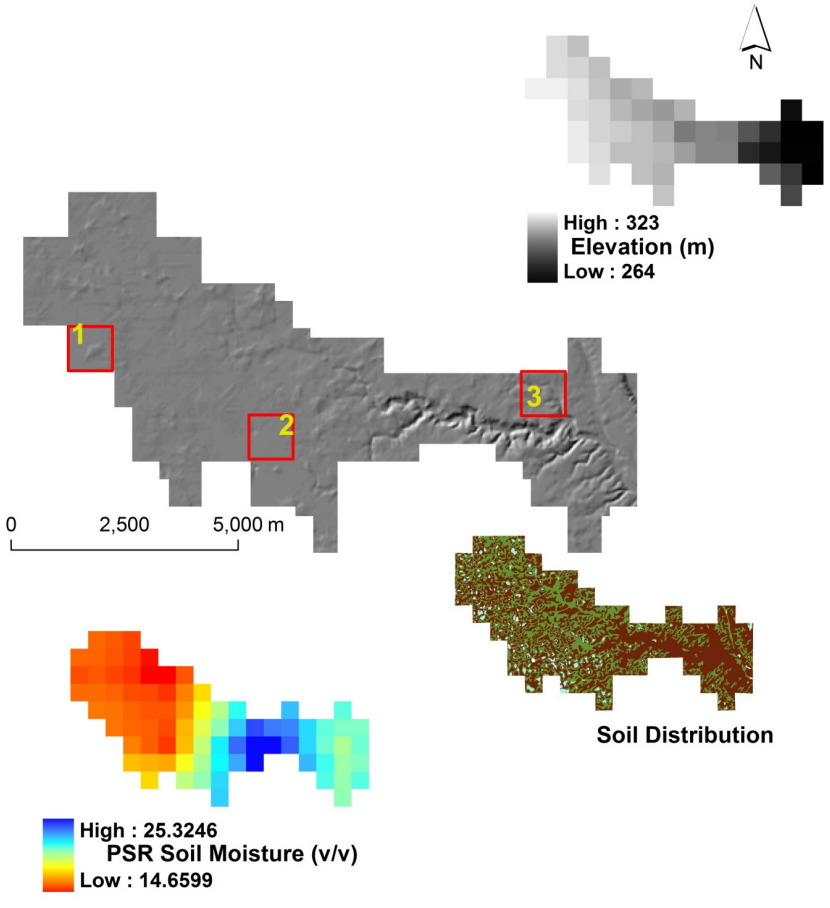

Figure 2. Walnut Creek watershed study area, location of selected pixels and some input layers for modeling.

Mohanty, 2012], combines the strengths of both the mean-type and the mode-type aggregation schemes. It is briefly reviewed here.

[10] The power average operator is defined as

$$P^*(p_1, p_2, \ldots, p_1) = \frac{\sum_{i=1}^{n}(1 + T(p_i))p_i}{\sum_{i=1}^{n}(1 + T(p_i))}, \quad (1)$$

where

$$T(p_i) = \sum_{\substack{j=1 \\ j \neq i}}^{n} \mathrm{Sup}(p_i, p_j). \quad (2)$$

P^* is the power average of the parameter values $p_i, \ldots, p_n$, where n is the total number of nodes being aggregated. $\mathrm{Sup}(p_i, p_j)$ is the support for p_i from p_j. This feature allows data clustered around a particular value to combine nonlinearly while being aggregated. A general form of the support equation is given by

$$\mathrm{Sup}(p_i, p_j) = e^{-\eta(p_i - p_j)^2}, \quad (3)$$

where $\eta \geq 0$. The value of η is given by the formula

$$\eta = \left(\frac{z_{j_{\max}} - z_{j_{\min}}}{z_i - z_j}\right)^2 * \frac{\sqrt{(x_i - x_j)^2 + (y_i - y_j)^2 + (z_i - z_j)^2}}{S}, \quad (4)$$

Here x, y, and z are the Cartesian coordinates of the point, while S is the scale (resolution) to which the hydraulic parameters are being aggregated. The first term on the right-hand side is the normalized difference in elevation between the two locations i and j. The second term provides the linear distance between measurement values, normalized by the scale dimension. As mentioned earlier, a more detailed description of the methodology is given in the article by *Jana and Mohanty* [2012].

2.3. Data Sets

[11] Elevation data for the LW and WC watersheds at 30 m resolution were obtained from the National Elevation Data set from the USDA-NRCS Geospatial Data Gateway [*http://datagateway.nrcs.usda.gov*]. From the same source, the National Land Cover Data set, and the Soil Survey spatial and tabular data (SSURGO) were also obtained for the LW region.

[12] Daily precipitation and stream discharge data for the LW watershed were obtained from the USDA-ARS Micronet database maintained by the Grazinglands Research Laboratory [*http://ars.mesonet.org/*] for the months of April–July 1997. Precipitation data from the 42 meteorological observation stations across the watershed were used to create daily precipitation maps by kriging. The corresponding precipitation value for each pixel was assigned as the time dependent boundary condition for the day. Daily temperature, relative humidity, and radiation values were also obtained from the USDA-ARS in order to compute the reference evapotranspiration (ET) for the region. ET was computed using the Penman-Monteith formula.

[13] Soil moisture data products from the electronically scanned thin array radiometer (ESTAR) for the LW region are available from the NASA-GSFC's Goddard Earth Sciences Data and Information Services Center [*http://daac.gsfc.nasa.gov/*]. The data were collected during the Southern Great Plains Hydrology Experiment 1997 (SGP97) using the L-band passive microwave ESTAR mapping instrument mounted on the NASA P-3 airplane. The sensor measures the microwave brightness temperatures, which are then converted to predict surface (0–5 cm) soil moisture estimates. The data are processed to produce georeferenced gridded products for each day of observation at a pixel resolution of 800 m. A detailed description of the ESTAR data and processing was given by *Jackson et al.* [1999]. The ESTAR soil moisture data product was used in this study to validate the outputs from the simulation of the LW domain using HYDRUS-3-D. ESTAR soil moisture data is available for 16 days in the period between mid-June and mid-July 1997 (DOY 169 to 197). This is the period during which the SGP97 hydrology experiment was conducted in the LW region.

[14] Data for the WC watershed were obtained from the National Snow and Ice Data Center (NSIDC) which is the repository for all data collected during the SMEX02 field experiments [*http://nsidc.org/data/amsr_validation/soil_moisture/smex02/index.html*]. Soil moisture data from the aircraft borne Polarimetric Scanning Radiometer (PSR) were used for this region at the coarse scale. The PSR instrument operates in the CX band, which is similar to the satellite borne AMSR sensors. The PSR data is available for a total of ten days between 25 June 2002 and 12 July 2002, during the SMEX02 campaign.

2.4. Physical Domain Setup

[15] The physically based HYDRUS-3-D hydrologic simulation software [*Šimůnek et al.*, 2006] was used to simulate the test domains for soil moisture and water fluxes. The HYDRUS-3-D software package solves the modified Richards' equation for water flow in saturated/unsaturated domains using numerical techniques and allows the user to analyze water flow through variably saturated regions with irregular boundaries and nonuniform soils. As the name suggests, HYDRUS-3-D allows for three-dimensional flow representations in the unsaturated zone. The governing equation (modified Richards' equation), the mathematical formulations of the boundary conditions, and other features of the HYDRUS-3-D model are explained in the companion paper [*Jana and Mohanty*, 2012], and are not repeated here.

[16] The entire watershed was divided into a grid of 1000 m × 1000 m pixels (Figure 1). Each of the pixels (672 for LW; 70 for WC) was simulated individually using the HYDRUS-3-D software. Elevation data at 30 m resolution were extracted for each grid block using a GIS software. The data were then fed to the HYDRUS-3-D platform for creating the geometry of the domain. A minimum soil depth of 6 m was maintained across all pixels. Corresponding soil textural properties data from the SSURGO database were extracted for each pixel and, using the ROSETTA [*Schaap et al.*, 2001] framework within HYDRUS-3-D, the corresponding soil hydraulic parameters for the van Genuchten-Mualem model with no hysteresis were obtained. These soil types were designated in the HYDRUS-3-D domain. Similarly, for each pixel domain, the land cover data were extracted and suitable root water uptake parameters were

assigned based on the vegetation. The Feddes model [*Feddes et al.*, 1978] for the root water uptake was applied in our study, with a maximum rooting depth of 1 m, and no osmotic stress. Water tables were assigned to the domain based on the location and landscape position in the watershed. Pixels close to the stream channel in the LW domain had water tables at 1 m, while those farthest from the stream were assigned water tables at 4 m depths. Similarly, for the WC domain, the water table was varied between 0.5 and 2 m.

[17] It has been reported by *Schilling and Helmers* [2008] that significant portions of agricultural land in Iowa are artificially drained by the use of subsurface tile drains. Based on their analysis of the Walnut Creek watershed, it was considered necessary to include the effect of the tile drains under the western third portion of the watershed. While it is known that the WC domain has an extensive network of these drains, no reliable information is available on their density and locations. Furthermore, implementation of the tile drain condition in the HYDRUS-3-D environment is currently not available for general (irregular) geometries. Hence, in order to approximate the effect of the tile drains, a sand layer was introduced into the HYDRUS simulations of each pixel domain in the western third of the watershed at a depth of 1 m from the surface. Since the sand layer is not a perfect representation of the tile drain network, certain assumptions and approximations are necessary. One of them deals with the flow direction. In a tile drain, water moves in only one direction laterally. This constraint of lateral anisotropy is not imposed in a sand layer. However, since the sand layer follows the surface topography, it may be reasonably assumed that the majority of the subsurface flow in this layer is downhill. This approximates the unidirectional lateral flow in the tile drain. A further limitation of the approximation is that the flow within the sand layer is not advective, as it would be within a tile drain. However, Darcian flow within the sand layer being a function of the hydraulic conductivity, the flow magnitude may not be much different since the sand has a high conductivity. The higher conductivity of the sand layer also forms a preferential flow path for the water in the lateral direction, thus limiting the vertical infiltration of water below the sand layer. This further approximates the effect of the tile drains. The sand layer was not part of the scaling algorithm, and was included only in the simulations.

[18] The version of HYDRUS-3-D available at the time of this study also did not account for surface runoff. This leads to downstream locations appearing drier than they actually are, due to the loss of the surface runon into those locations. Hence, an algorithm to capture the effect of the runoff/on process, and to update the soil moisture states of the pixels based on this information was applied. In a GIS environment, using the elevation data, the flow direction out of each pixel was computed using a *d-inf* algorithm [*Tarboton*, 1997]. The amount of runoff generated by each pixel during the one day simulation was computed as the difference between the precipitation volume over the pixel domain and the infiltration into the domain. This amount of water was routed to the downstream pixel based on the flow direction map (Figure 3). The runon volume to the downstream pixel was distributed across the entire area and the surface soil moisture state of the downstream pixel updated to reflect the increased water content in the domain. Also, subsurface flux connections between pixels were implemented on the seepage faces. Seepage face boundary conditions allow for the removal of water from the saturated portions of the domain boundary. At each

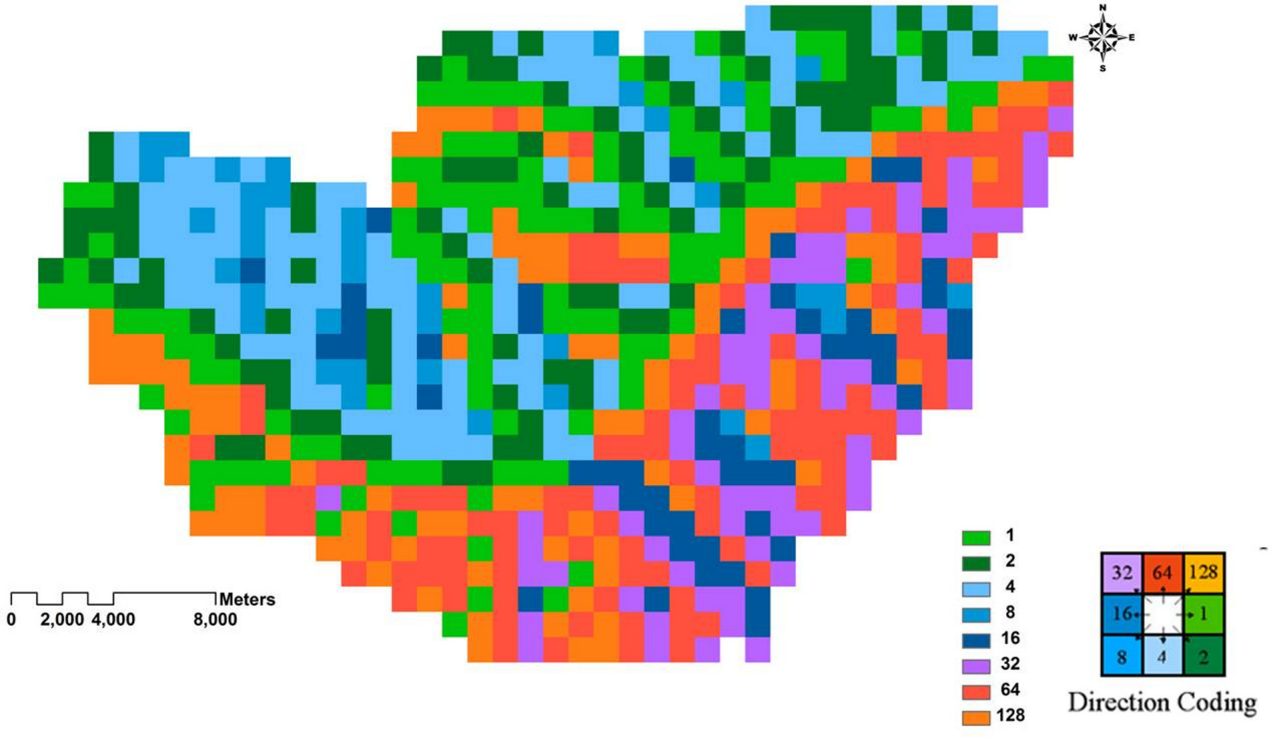

Figure 3. Flow routing map for the Little Washita watershed at 1 km resolution.

cross-sectional boundary, the two adjacent pixels were compared to determine which one had the higher water table at each daily time step. Then, the volume of water ejected from only those nodes above the water table of the adjacent pixel was computed. This volume was then distributed among the unsaturated nodes on the seepage face of the pixel with the lower water table. This simulates flow from a higher water table level to a lower one on a daily time step.

[19] All pixels making up the watershed domain were individually simulated for one day (at a time) with a minimum time step of 0.5 h. At the end of the daily time step, the surface and subsurface moisture states of each pixel were updated for surface runoff/on and seepage as described above. Once all pixels had been updated, they were then simulated for the second day, and the process repeated. The simulation was run for three months—from mid-April 1997 to mid-July 1997 for LW, and mid-April 2002 to mid-July 2002 for WC. The first two months were considered as the model spin-up time to allow the domain characteristics to stabilize, and only the last 1 month was used in the analysis.

[20] Finite element meshes were generated for each pixel with 20 horizontal layers and node spacings of 30 m. The top surface was assigned a time-dependent atmospheric boundary condition, while the vertical cross sections across the periphery of soil plot were designated as seepage faces to enable lateral flow of water through the soil domain. The lower boundary had a variable head boundary condition depending on the depth to the water table. Initial conditions of the soil profile were given by soil water contents just under saturation for the domain since a significant precipitation event occurred immediately before the commencement of the simulations.

[21] Initially, each node in the FEM was assigned a soil type based on the SSURGO data. The aggregation algorithm, described in section 2.2, was applied to upscale the five soil hydraulic parameters—residual soil water content (θ_r); saturation water content (θ_s); van Genuchten parameters α and n; and the saturated hydraulic conductivity K_s. These parameters were aggregated from 30 m to the 1 km resolution. Rather than coarsening the FEM grid, we assigned the aggregated effective soil hydraulic parameters to each node within the upscaled pixel footprint. This was done so that the computational integrity of the FEM would be consistent across all scales. It must be noted that while the soil types or hydraulic parameter values were assigned to the FEM nodes, the HYDRUS program interpolates the values to the 3-D elements (volume) in the mesh. The pixel domains with the upscaled soil hydraulic parameters were then put through the same simulation and soil moisture updating procedure as before.

[22] The five soil hydraulic parameters (θ_r, θ_s, α, n, and K_s) were upscaled using the power averaging operator from 30 m resolution to 1 km resolution for all 672 pixels in the Little Washita watershed domain and 70 pixels in the Walnut Creek domain. Twelve pixels of 1 km $\times$ 1 km size were selected from across the LW watershed for analysis, based on their landscape position, topography, land cover, and soil type so as to encompass the variety in the watershed, as shown in Figure 1. Three coarse resolution pixel domains were selected in the WC watershed for analysis.

Table 1. Elevation, Land Cover, and Compound Topographic Index (CTI) Details of Selected Pixels in the Watershed Domains

		Average Elevation (m)	Land Cover	Average CTI	Water Table (m)
LW	Pixel 1	446	Pasture	7.332	4
	Pixel 2	355	Pasture	7.312	1
	Pixel 3	369	Pasture	6.656	2
	Pixel 4	408	Bare	6.846	3
	Pixel 5	410	Bare	6.846	2
	Pixel 6	345	Wheat	7.379	1
	Pixel 7	341	Wheat	7.396	2
	Pixel 8	407	Bare	7.128	4
	Pixel 9	392	Pasture	6.709	3
	Pixel 10	419	Wheat	7.274	3
	Pixel 11	377	Pasture	7.085	2
	Pixel 12	394	Pasture	7.247	3
WC	Pixel 1	323	Corn		2
	Pixel 2	314	Soybean		1
	Pixel 3	287	Corn		0.5

Table 1 shows the average elevation (at 1 km resolution), land cover, and water table values for the selected pixels.

[23] In the LW watershed, except for pixel 4, all other pixels had at least three different soil types distributed in the pixel, as shown in Figure 4. In the WC watershed, all three pixels had three different soil types distributed within them.

[24] Average daily surface soil moisture states were compared for the LW pixels for the 16 days on which the ESTAR data product is available. Based on the ESTAR soil moisture data, the days with soil moisture greater than 0.20 (v/v) were designated "wet" days, while those with less than 0.10 (v/v) were designated "dry" days, with the "intermediate" days when soil moisture values were in between the 0.10 and 0.20 (v/v). In the WC watershed, PSR soil moisture data was available for 10 days. Based on the available data, days with soil moisture greater than 0.28 (v/v) were considered "wet" days and those with soil moisture less than 0.19 (v/v) as "dry" days for this region.

[25] In order to compare the model outputs, we used Pearson's correlation coefficient (R) and the root mean squared error (RMSE) as the main metrics. Pearson's correlation coefficient is computed as

$$R_{X,Y} = \frac{\mathrm{cov}(X, Y)}{\sigma_X \sigma_Y}, \tag{5}$$

where cov is the covariance between the two quantities being compared (X and Y), and σ is the standard deviation. The RMSE is computed as

$$RMSE_Y = \sqrt{E\left((Y - X)^2\right)}, \tag{6}$$

where E is the expected value of the square of the difference between Y and X. We used Pearson's R as the comparison metric since we were interested in knowing how the variability in the simulated fluxes and states related with the observed data. Rather than trying to reach a deterministic value for the fluxes and states, we wanted to capture the variability with respect to the controlling factors. Hence the focus on the correlation. In all discussions for the remainder

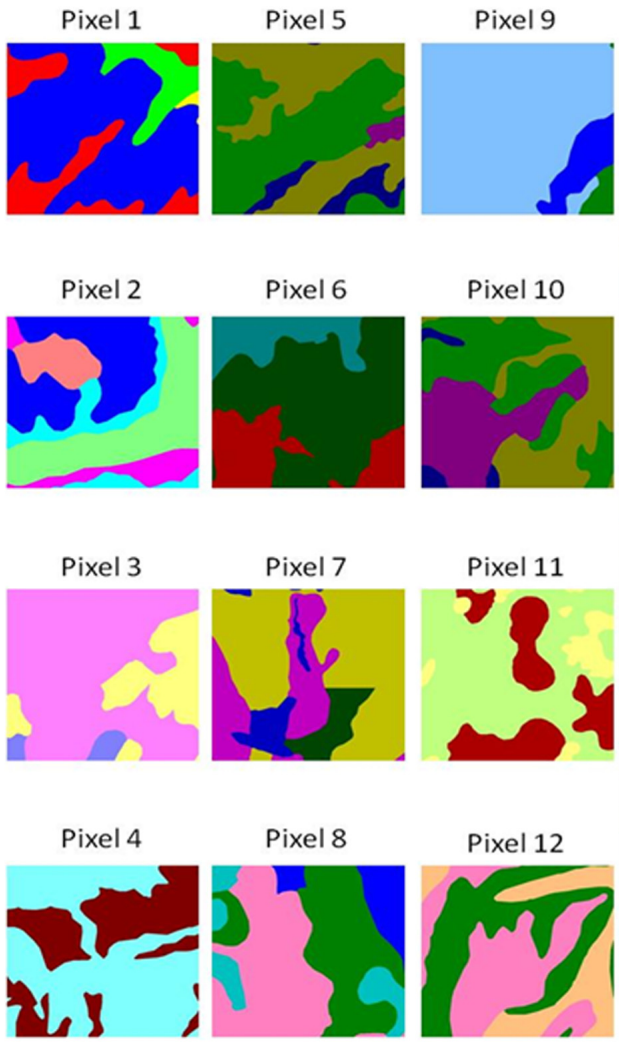

Soil Category	θr (v/v)	θs (v/v)	α (1/cm)	n (-)	Ks (cm/day)
1	0.034	0.302	0.007	1.340	1.099
2	0.028	0.274	0.018	1.260	2.391
3	0.030	0.273	0.023	1.254	3.119
4	0.037	0.304	0.005	1.291	0.221
5	0.038	0.307	0.004	1.337	0.229
6	0.052	0.505	0.020	1.347	100.032
7	0.020	0.269	0.021	1.324	11.644
8	0.031	0.274	0.023	1.244	2.390
9	0.023	0.271	0.039	1.359	39.312
10	0.050	0.512	0.021	1.327	102.153
11	0.020	0.261	0.028	1.311	9.626
12	0.034	0.297	0.005	1.308	0.348
13	0.021	0.268	0.027	1.321	15.125
14	0.035	0.301	0.003	1.408	0.295
15	0.035	0.300	0.004	1.348	0.291
16	0.040	0.318	0.005	1.317	0.466
17	0.082	0.539	0.028	1.302	70.970
18	0.052	0.503	0.019	1.356	82.319
19	0.058	0.513	0.019	1.344	86.635
20	0.043	0.326	0.006	1.218	0.121
21	0.051	0.505	0.020	1.341	97.556
22	0.033	0.262	0.040	1.274	6.761
23	0.036	0.270	0.034	1.246	2.864
24	0.032	0.276	0.022	1.234	1.877
25	0.037	0.300	0.006	1.312	0.495
26	0.032	0.274	0.023	1.229	1.702
27	0.031	0.288	0.005	1.369	0.637
28	0.040	0.319	0.005	1.319	0.432

Figure 4. Soil distributions in the 12 selected pixels in LW. Different colors represent different soils.

of this article, the term "correlation" will refer to the Pearson's correlation coefficient R. The RMSE, on the other hand, provides information regarding the bias in the simulation outputs with respect to the observations. While the simulated and observed values may be highly correlated, a large bias can put the values far apart from each other, thus signifying poor model estimation. Hence, for a model to be accepted as performing well, the value of R should be high (ideally 1) and RMSE should be low (ideally 0).

3. Results and Discussion

[26] As stated earlier, the primary objective of the study was to obtain effective upscaled values of soil hydraulic parameters such as the saturated hydraulic conductivity, the saturation and residual soil water contents, and the van Genuchten parameters, at the 1 km × 1 km domain/pixel size (hillslope scale) for entire watersheds while incorporating the influence of the local topography into the scaling algorithm. Here we discuss the performance of the scaling algorithm and the hydrologic simulation model with regard to specific research questions which provide evaluations of the scaling algorithm to meet the stated objectives.

3.1. Does the Topography-Based Scaling Algorithm Provide Effective Coarse Resolution Soil Hydraulic Parameters With Respect to Soil Moisture?

[27] In section 3.1 we discuss the performance of the topography-based scaling algorithm in providing effective coarse resolution soil hydraulic parameters. To be considered effective, the coarse resolution parameters should generate the same soil moisture states and fluxes as those at the fine resolution. Table 2 shows the Pearson's correlations (R) and the RMSE between the average daily surface soil moisture states of the selected analysis pixels as obtained using fine scale and upscaled soil hydraulic parameters in the HYDRUS-3-D simulation software. Overall, a high correlation was obtained between the fine and coarse scale simulated soil moistures at both test sites. It was seen that for most of the pixels with significant number of wet days in the LW watershed, the correlations were better without the runoff routing. This could be due to the updating of soil moisture states leading to an overprediction of the next day's state, as compared to the no-routing methodology. It was seen that the flow routing algorithm implemented in the study improved the correlations for the drier pixels. It

Table 2. Comparison Between Fine and Coarse Scale Simulated Soil Moistures for Selected Pixels[a]

			R (w/o Runoff Routing)					*R* (With Runoff Routing)			
		RMSE (w/o Runoff)	Overall	Wet	Inter	Dry	RMSE (With Runoff)	Overall	Wet	Inter	Dry
LW	Pixel 1	0.098	0.96[b]	0.93[b]	0.83[b]		0.024	0.92[b]	0.85[b]	0.93[b]	
	Pixel 2	0.051	0.94[b]	0.89[b]	0.83[b]		0.035	0.91[b]	0.86[b]	0.86[b]	
	Pixel 3	0.097	0.94[b]	0.87[b]	0.84[b]		0.030	0.92[b]	0.87[b]	0.86[b]	
	Pixel 4	0.068	0.90[b]		0.82[b]		0.025	0.88[b]		0.89[b]	
	Pixel 5	0.098	0.95[b]	0.88[b]	0.89[b]		0.021	0.93[b]	0.95[b]	0.86[b]	
	Pixel 6	0.087	0.90[b]		0.91[b]		0.039	0.94[b]		0.86[b]	
	Pixel 7	0.094	0.84[b]		0.92[b]	0.87[b]	0.045	0.93[b]		0.81[b]	0.94[b]
	Pixel 8	0.061	0.95[b]		0.84[b]	0.77[b]	0.046	0.96[b]		0.89[b]	0.89[b]
	Pixel 9	0.092	0.92[b]		0.78[b]		0.038	0.88[b]		0.85[b]	
	Pixel 10	0.061	0.66[c]	0.83[b]	0.72[c]		0.030	0.73[c]	0.85[b]	0.81[b]	
	Pixel 11	0.053	0.87[b]		0.80[b]		0.049	0.88[b]		0.82[b]	
	Pixel 12	0.094	0.87[b]		0.83[b]	0.83[b]	0.039	0.87[b]		0.80[b]	0.93[b]
WC	Pixel 1	0.030	0.96[b]	0.98[b]	0.86[b]	0.89[b]	0.033	0.94[b]	0.87[b]	0.92[b]	0.93[b]
	Pixel 2	0.037	0.98[b]	0.89[b]	0.89[b]	0.89[b]	0.026	0.96[b]	0.88[b]	0.72[b]	0.94[b]
	Pixel 3	0.047	0.95[b]	0.98[b]	0.86[b]	0.96[b]	0.055	0.93[b]	0.95[b]	0.94[b]	0.93[b]

[a]RMSE: root mean square error (vol/vol); *R*: Pearson's correlation coefficient.
[b]Correlations significant at the 0.01 level.
[c]Correlations significant at the 0.05 level.

was observed that the average soil moisture values obtained with runoff routing were consistently higher than those without the routing. The average soil moistures (across all observation days) for each pixel are plotted in Figure 5. As also shown by the better correlations, the differences in variability between the fine and coarse scale simulated soil moistures were much smaller when the runoff routing was implemented. However, it was observed that the range of soil moisture values across the observation period for each pixel, represented by the error bars on the plot, was larger with the routing implementation. This could be an artifact of the routing algorithm by introducing a lag in the response times of the domain.

[28] At the WC site, all three selected pixels had wet, intermediate, and dry days. Similar to the LW site, the average soil moisture for all three pixels were consistently higher for the case with runoff routing, at both scales. However, no significant differences in correlations were observed between the two cases (Table 2). The average soil moisture values for the three selected pixels in the WC watershed are plotted in Figure 6.

[29] The high correlations between the fine and coarse scale simulated soil moistures at both test locations are indications that the upscaling scheme applied to aggregate the fine scale soil hydraulic parameter values is providing an effective set of parameters at the coarse scale.

3.2. Do the Upscaled Soil Hydraulic Parameters Result in Soil Moisture States That Reflect Reality?

[30] In section 3.2 we compare the coarse resolution simulated soil moisture states to field observations from airborne remote sensors. This provides an estimate of the performance of the upscaling algorithm and the hydrologic simulation model with regard to producing outputs that match field data. While the previous subsection provides insight into the performance of the scaling algorithm with respect to providing effective coarse resolution parameters, the ultimate test of applicability of the algorithm in practice is in how well the simulated soil moisture states match the observations. In order to test this, the coarse scale simulated soil moistures were compared with the remotely sensed ESTAR/PSR soil moisture data products, which were resampled to the 1 km resolution from 800 m. The average daily soil moisture values from the ESTAR sensor are plotted in Figure 7 against the simulated soil moisture generated with runoff routing for the 12 selected pixels in the LW watershed. It was seen that, while the simulated soil moisture values were slightly overestimated in most cases, in general, the simulated soil moisture values were clustered close to the 1:1 line. This signifies that the simulated soil moisture values are close to the ESTAR-measured values. Correlations of the simulated soil moisture values with the ESTAR measured soil moisture for the 12 analysis pixels in the LW watershed are presented in Table 3. Again, a high degree of correlation was found between the observed ESTAR soil moisture and the simulated values. A histogram of the correlations between the simulated soil moisture generated with runoff routing and the ESTAR measurements was plotted (Figure 8) for all 672 pixels in the LW watershed. It was seen that the distribution was skewed toward the higher correlation values, with an average value of 0.85 for the entire watershed.

[31] It was seen that the runoff routing generated consistently better estimates of the surface soil moisture for all pixels, across wet, intermediate, and dry days. The correlations between the simulated and ESTAR soil moisture ranged between 0.73 and 0.76 for the wet days when no runoff routing was implemented. The range improved to 0.76–0.83 when the routing algorithm was applied. The overall correlation of pixels with significant wet days was also improved by the runoff routing. This is a marked difference from the observation in section. 3.1 This implies that it is in fact the fine scale soil moisture values that were underpredicted, and not an overprediction when using the coarse scale effective hydraulic parameters, as previously mentioned in section 3.1.

[32] While there would be little routing of surface fluxes on most intermediate, and all dry days, it was seen that the application of the runoff routing algorithm still improved the performance on those days. The routing scheme ensured

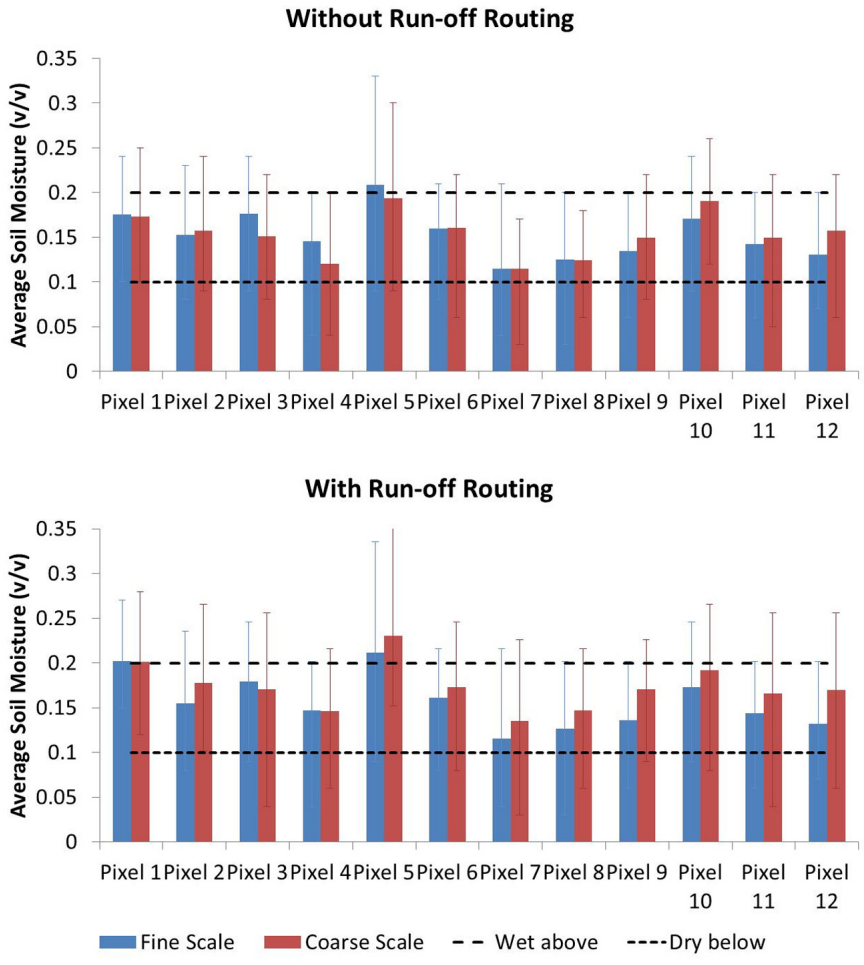

Figure 5. Average simulated fine and coarse scale soil moistures of selected pixels in LW watershed. Error bars represent variation across time for each pixel.

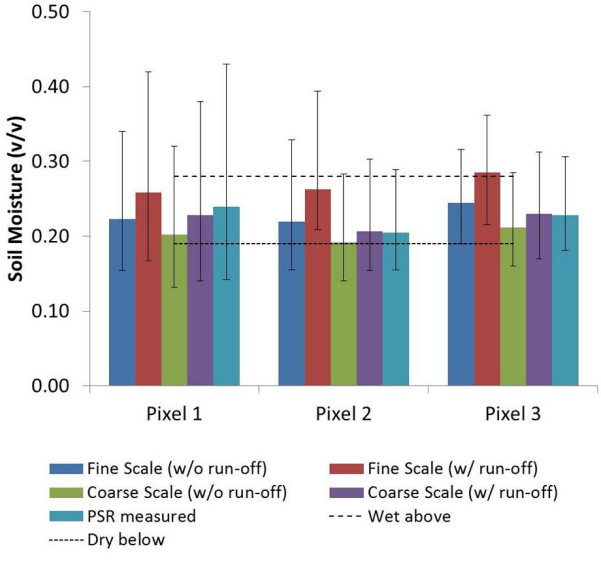

Figure 6. Average simulated fine and coarse scale soil moistures of selected pixels in WC watershed, along with PSR measured data. Error bars represent variation across time for each pixel.

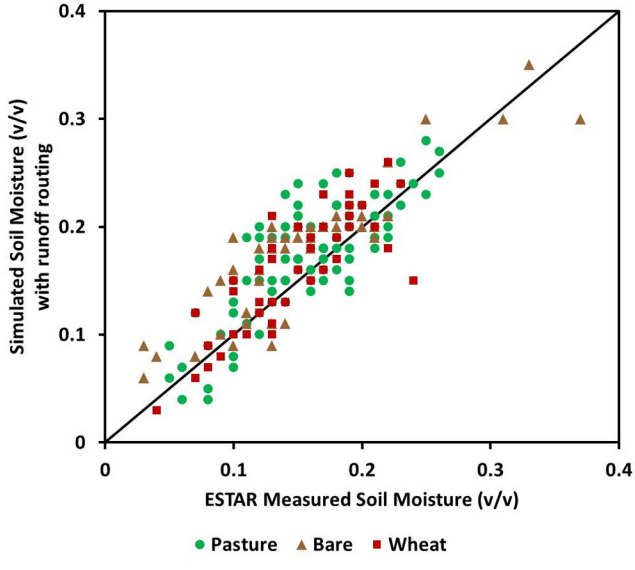

Figure 7. ESTAR measured, and simulated soil moisture (with runoff routing) values for the 12 selected pixels in LW watershed.

Table 3. Comparison Between Coarse Scale Simulated Soil Moisture and Remote Sensing Observations[a]

		Average Elevation (m)	Land Cover	Average CTI	Variance CTI	Water Table (m)	RMSE (w/o Runoff)	*R* (w/o Runoff Routing) Overall	Wet	Inter	Dry	RMSE (With Runoff)	*R* (With Runoff Routing) Overall	Wet	Inter	Dry
LW	Pixel 1	446	Pasture	7.332	1.15	4	0.066	0.87[b]	0.74[c]	0.66[c]		0.043	0.89[b]	0.81[b]	0.72[c]	
	Pixel 2	355	Pasture	7.312	1.43	1	0.047	0.88[b]	0.76[b]	0.69[c]		0.041	0.91[b]	0.83[b]	0.77[b]	
	Pixel 3	369	Pasture	6.656	0.82	2	0.050	0.88[b]	0.73[c]	0.68[c]		0.035	0.89[b]	0.80[b]	0.76[b]	
	Pixel 4	408	Bare	6.846	0.81	3	0.047	0.82[b]		0.69[c]		0.040	0.82[b]		0.70[c]	
	Pixel 5	410	Bare	6.846	1.21	2	0.047	0.89[b]	0.73[c]	0.67[c]		0.042	0.90[b]	0.80[b]	0.75[c]	
	Pixel 6	345	Wheat	7.379	1.67	1	0.045	0.76[b]		0.67[c]		0.038	0.84[b]		0.77[b]	
	Pixel 7	341	Wheat	7.396	1.41	2	0.040	0.75[c]		0.67[c]	0.62[c]	0.034	0.84[b]		0.72[c]	0.65[c]
	Pixel 8	407	Bare	7.128	1.70	4	0.064	0.88[b]		0.67[c]	0.64[c]	0.022	0.89[b]		0.75[c]	0.65[c]
	Pixel 9	392	Pasture	6.709	0.89	3	0.068	0.84[b]		0.67[c]		0.035	0.89[b]		0.76[b]	
	Pixel 10	419	Wheat	7.274	0.90	3	0.043	0.67[c]	0.76[b]	0.66[c]		0.032	0.71[c]	0.76[b]	0.76[b]	
	Pixel 11	377	Pasture	7.085	1.44	2	0.064	0.76[b]		0.67[c]		0.039	0.81[b]		0.75[c]	
	Pixel 12	394	Pasture	7.247	1.57	3	0.065	0.84[b]		0.69[c]	0.61[c]	0.024	0.82[b]		0.71[c]	0.68[c]
WC	Pixel 1	323	Corn			2	0.055	0.96[b]	0.76[b]	0.98[b]	0.84[b]	0.035	0.96[b]	0.84[b]	0.85[b]	0.78[b]
	Pixel 2	314	Soybean			1	0.049	0.94[b]	0.98[b]	0.77[b]	0.83[b]	0.043	0.95[b]	0.98[b]	0.84[b]	0.80[b]
	Pixel 3	287	Corn			0.5	0.046	0.83[b]	0.63[b]	0.85[b]	0.81[b]	0.041	0.86[b]	0.72[b]	0.79[b]	0.86[b]

[a]RMSE: root mean square error (vol/vol); *R*: Pearson's correlation coefficient.
[b]Correlations significant at the 0.01 level.
[c]Correlations significant at the 0.05 level.

that a more realistic distribution of soil moisture was obtained in downstream pixels due to the updating of the values at daily time steps to reflect the inflow into the pixel from upstream pixels. On dry days, when there was no surface flux to be routed downstream, the downstream pixels already had a better estimate of the actual soil moisture from the previous time steps, as against the case where the routing was never applied. Hence, this history of soil moisture updating helped the pixel to be better correlated with the ESTAR observed value even on dry days. It was observed that during the initial drying phase, the modeled soil moisture was mostly overpredicted by a small amount, as compared with the ESTAR data. However, during the subsequent wetting phase, this pattern was not seen.

[33] Correlations between the simulated coarse resolution soil moisture and the PSR observations at the WC location are also given in Table 3. While there was little difference in the correlations between the PSR observations and the coarse scale simulated soil moistures with or without runoff routing, it can be seen from Figure 6 that the runoff routing brought the numerical values of the simulated soil moisture fields closer to the observations.

3.3. Does the Performance of the Scaling Algorithm Vary With Changes in Specific Factors?

[34] In section 3.3 we evaluate the performance of the scaling algorithm varies with changes in physical factors such as location, elevation, topographic complexity, and land cover. For a scaling algorithm to be considered a generic one, it is necessary that the performance not vary much with changes in these factors.

3.3.1. Location and Elevation

[35] Precipitation data from the 12 meteorological stations closest to the selected pixels in the LW watershed are plotted in Figure 9. It can be seen that while the precipitation amounts varied across the watershed, a significant

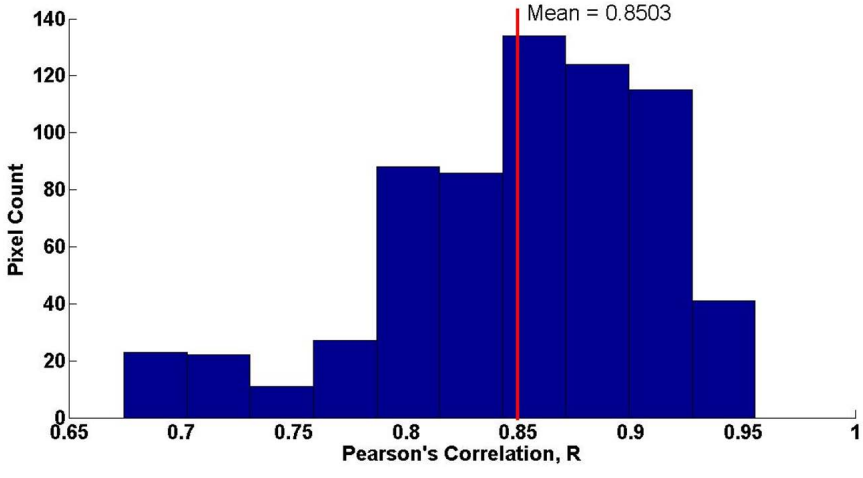

Figure 8. Histogram of Pearson's correlation between coarse scale soil moisture simulated with runoff and ESTAR measurements for all 672 pixels in LW watershed.

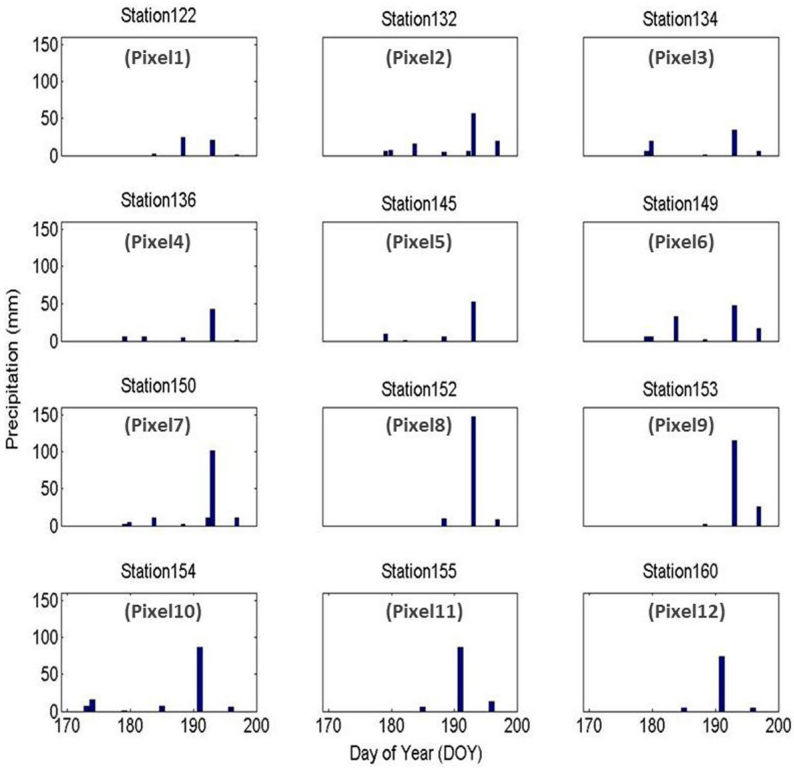

Figure 9. Precipitation data from twelve meteorological observing stations close to the selected pixels in LW watershed.

event occurred around DOY 191 across the entire watershed. Based on the precipitation patterns, it was also observed that the western portion of the watershed received more rainfall as compared to the eastern parts. However, no significant difference in the performance of the upscaling algorithm was observed based on the location of the pixel within the watershed. Table 3 shows the correlation coefficients between the simulated and ESTAR measured soil moisture and the average elevation of the pixel at the 1 km resolution. It is also to be noted that pixels 2, 3, 6, and 7, which have the lowest elevations, were situated in the eastern part of the watershed. Pixels 1, 4, 5, and 10, having the highest elevations, were located in the western portion of the LW watershed, while the remaining four pixels (8, 9, 11, and 12) were in the middle portion. It may be observed that none of the pixels in the middle portion had a significant number of wet days, while two of the three pixels with significant number of dry days were in this region. The fact that the western portion received more rainfall than the east is also verified by most number of pixels with significant number of wet days being in this portion. Pixel 5, which exhibited the most number of wet days, was the westernmost pixel selected for analysis. Downstream pixels 2 and 3, which also exhibit higher soil moisture states, were located close to the streambed. This would mean that the influx of water by surface runoff into these pixels was significantly more than the others located at higher elevation, which was reflected in the higher soil moisture values.

[36] In the WC region, the streamflow direction was again generally from west to east. The western portion of the watershed, in this case, was generally drier than the eastern portion. This could be due to the presence of subsurface tile drains in this portion of the watershed. The WC watershed is a much smaller catchment as compared to the LW watershed and the variations in precipitation patterns across the watershed were negligible. Hence, the variation in soil moisture across the watershed may be attributed to the drainage of the water toward the stream channel in the east. Although pixel 1 is in the western portion of the watershed, pixel 2 in the middle, and pixel 3 in the east, no difference was noticed in the performance of the upscaling algorithm.

3.3.2. Topographic Variations

[37] Compound topographic indices $[\ln(A/\tan(B))]$ [*Beven et al.*, 1984; *Kirkby*, 1975] were computed for each of the 12 pixels using the fine scale (30 m) elevation data. It has been reported by *Pradhan et al.* [2006] that the grid resolutions of the DEMs used to compute the topographic index have a significant influence on the reliability of the CTI values. As coarser grids are used, the reliability reduces. This is attributed to the fact that the higher resolution topographic characteristics are smoothed out and lost when coarse resolution DEM's are used. Hence, we used the fine scale (30 m) DEM to compute the CTI. The "*dinf*" algorithm suggested by *Tarboton* [1997] was used to compute the flow direction, and thus the upslope contributing area for the compound topographic index (CTI). This algorithm has been shown to provide more realistic representations since the flow directions are not fixed, and flow can occur in multiple directions.

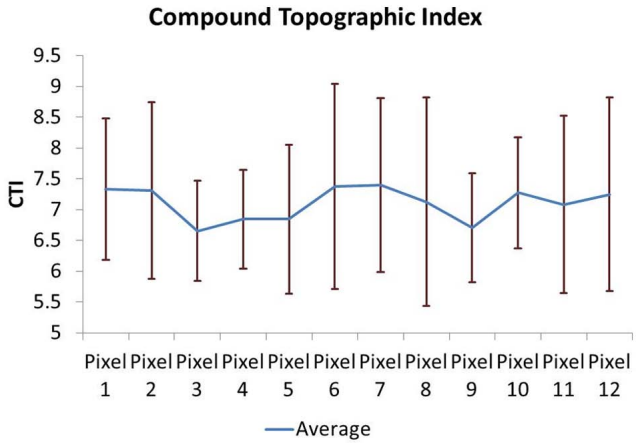

Figure 10. Average compound topographic index of 12 selected pixels in LW watershed derived from 30 m resolution DEM. Error bars represent the variance of CTI within each pixel.

[38] The average and variance of the CTI values within each of the 12 analysis pixels were computed. The average and variance of the CTI at each pixel are plotted in Figure 10. It can be seen that while there was only a small variation in the average CTI value among the pixels, the distribution within each pixel, represented by the error bars, varied more significantly. This signified that while at the coarse resolution, all the pixels appeared to be similar with respect to the CTI, at the finer resolution, there were big differences. Correlations of the average CTI with the simulated and ESTAR measured surface soil moisture distributions were computed across all the pixels. These are reported in Table 4. It is immediately apparent that there was no significant correlation between the soil moisture pattern and the CTI. This finding is in line with those of *Western et al.* [1999] and *Jana and Mohanty* [2012] who reported that the wetness index was found to be a very poor predictor of soil moisture spatial variability. The ESTAR measured and simulated soil moisture values appeared to be slightly better correlated with the standard deviation, or variance, of the CTI within each pixel. However, this was not a significant relationship. Table 3 shows the average CTI and the variance in CTI besides the correlation coefficients between the simulated and ESTAR soil moisture values. It was seen that most of the pixels with significant number of wet days had lesser variation in the CTI.

[39] Correlations between the CTI and the upscaled soil hydraulic parameters were also computed (Table 5). While no significant relationship could be deduced from this table,

Table 4. Correlations Between Average and Variance of Compound Topographic Index (CTI), and Soil Moisture Values Across All Pixels in LW Watershed

		ESTAR SM	Simulated SM With Runoff	Simulated SM w/o Runoff
CTI	Average	−0.093	−0.082	0.041
	Std. Dev.	−0.335	−0.150	−0.134
	Variance	−0.360	−0.176	−0.155

Table 5. Correlations Between Upscaled Soil Hydraulic Parameters and CTI Across All Pixels in LW Watershed

		Upscaled Soil Hydraulic Parameters				
		θ_r	θ_s	α	n	K_s
CTI	Average	−0.138	−0.195	−0.167	0.409	0.001
	Std. Dev.	−0.392	−0.379	0.289	0.264	0.224
	Variance	−0.414	−0.401	0.289	0.287	0.229

the soil hydraulic parameters showed better correlation with the average CTI in general. Here again, the variance in CTI was better correlated over the average for most parameters. The van Genuchten parameter n showed the best correlation with the average CTI.

3.3.3. Land Cover

[40] Table 3 shows the correlation coefficients between the ESTAR observed and simulated soil moistures along with the land cover within the LW pixel. It was seen that the pasture pixels had the best overall correlations, followed by the bare pixels. The pixels with a winter wheat cover showed the least correlation between the simulated and ESTAR measured soil moistures. This could be due to crop management practices such as harvesting, or water logging taking place during this period, which have not been accounted for in our study. Furthermore, it was seen that most of the pixels with significant wet days had a pasture cover. The pixel with most wet days (pixel 5) had a bare soil cover.

[41] From Figure 7 it was seen that the simulated soil moisture for all three land cover types in the LW watershed were close to the ESTAR measurements. The variation of standard deviation of soil moisture versus the mean soil moisture, classified on the land cover is plotted in Figure 11. Following the methodology used by *Famiglietti et al.* [2008], the standard deviations were averaged within bins of width 0.05 v/v of mean soil moisture. While the wheat pixels displayed a "concave-upward" shape as found by *Famiglietti et al.* [2008], the pasture and bare land cover

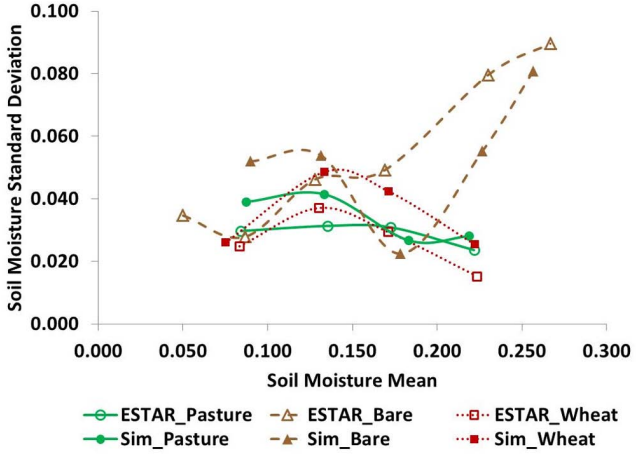

Figure 11. Standard deviations of soil moisture classified on the land cover. The standard deviations are averaged within bins of width 0.05 v/v of mean soil moisture.

pixels did not entirely conform to this shape. In the Little Washita watershed, the wheat fields tend to be those that have relatively little topographic relief, as compared to the pasture/bare fields. This observation is supported by analysis of the CTIs of the pixels. Over all 672 pixels in the LW watershed, the pixels with a pastureland cover had an average CTI of 7.018 and a standard deviation of 1.142. An index of topographic simplicity can be computed as the mean CTI divided by the standard deviation. This simplicity index provides an estimate of how the CTI varies with regard to its mean value. High values of the index mean that there is little variation across fields and the CTI is high. This means consistent low topographic complexity. The computed simplicity index for the pastureland cover pixels was 6.145. Similarly, for the bare pixels, the CTI mean, CTI standard deviation, and simplicity index were 6.956, 1.002, and 6.939 respectively. The corresponding values for the wheat pixels were 7.270, 0.633, and 11.477. The high simplicity index values for the wheat pixels indicated that they displayed simpler topographies. The topographic complexity of the pasture and bare pixels could be the reason for the soil moisture from those pixels to deviate from the parabolic shape. Topography causes ponding of surface water at the valleys, and also subsurface soil moisture dynamics toward the lower elevations. This causes the soil profile to generally be drier near the crest, than at the valley. While the overall mean soil moisture for the pixel could be high, the variability was also not reduced. In a flatter terrain, such as a wheat field, there is no topographically driven surface or subsurface localizing of soil moisture, thus reducing the variability at the higher end of the soil water retention curve. Hence, while the variations shown in Figure 10 appear to be land cover specific, they could very well be caused by the underlying topographic differences.

[42] While pixels 1 and 3 of the WC watershed have a corn vegetative cover, pixel 2 has soybean (Table 1). Pixel 2 can also be considered to be mostly bare since the soybean plant does not cover much area. This is especially true at the beginning of the analysis period when the plant is very small. However, these vegetation differences did not seem to affect the upscaling performance of the power averaging operator used in this study.

[43] It has been previously hypothesized [*Jana and Mohanty*, 2012] that different physical controls dominate soil property and moisture variability at different scales. It is thought that the soil texture and structure dominate at the smaller scales, while topography exerts more influence at hillslope (kilometer) scales. Beyond that, at regional scales, the vegetation or land cover may be the dominant control, leading to the controls exerted by regional climate. The distinct differences in the correlations based on the land cover suggest that the vegetation is exerting some influence on the soil moisture variation at the hillslope scale too.

3.4. Does the Scaling Algorithm Provide Effective Coarse Resolution Soil Hydraulic Parameters With Respect to Streamflow?

[44] Apart from the soil moisture states, effective soil hydraulic parameters must also result in comparably similar fluxes at the coarse resolution. In order to evaluate the performance of the topography-based scaling algorithm with regard to fluxes, stream discharge data from the USGS stream gauges (Figure 1) were used to compare the flux from the HYDRUS-3-D simulations of the LW domain. The upstream gauge, SG442, was located close to pixel 5, while the downstream gauge, SG447, was located close to pixel 9. Surface flux outputs from those pixels that drained into the pixel with the stream gauge were summed up and matched with the stream discharge recorded at the two gauges daily. It was intended to use another stream gauge near the watershed outlet for further analysis, but unfortunately none of the gauges near the outlet were functional during the period of analysis. Hence only two gauges were used.

[45] Figure 12 shows the plot of the stream discharge as measured at SG442, along with the flux output from pixel 5 (model). The green box represents the analysis period between mid-June and mid-July 1997. It was observed that the model flux had a very poor correlation with the measured discharge. However, upon accounting for a response time lag of one day, the correlations improved significantly.

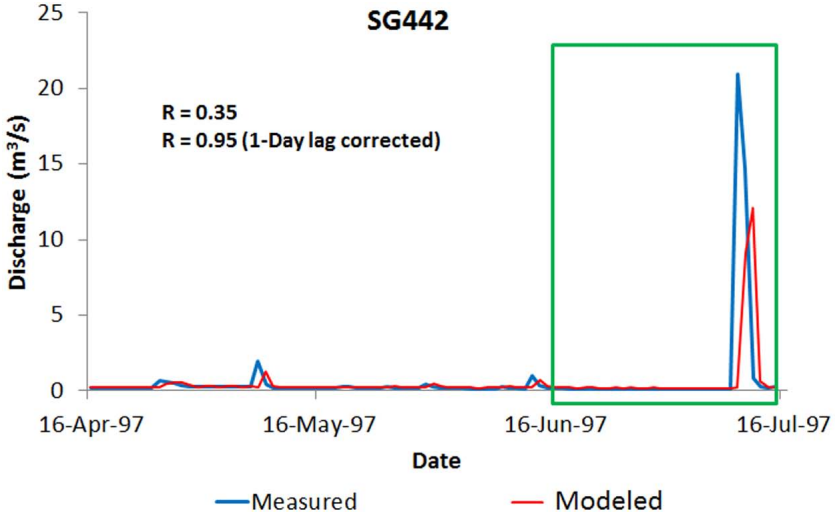

Figure 12. Stream discharge measured at upstream gauge SG442 in LW watershed.

This time lag could be attributed to the nature of the runoff routing algorithm implemented in this study. We computed the surface flows at the end of each daily time step, and then updated the soil moisture state as initial condition for the next day. This means that although there may have been a precipitation event in the morning of a particular day, and in reality the runoff reached the downstream pixel the same day, our routing algorithm accounted for this only the next day. Hence, a response time lag was seen.

[46] Figure 13 shows a similar plot of discharge at the downstream gauge, SG447, and corresponding surface flux from pixel 9. In this case, a two-day response time lag was observed. On accounting for the time lag, it was seen that the correlation again improved significantly. SG442, being upstream, has a lesser number of pixels draining into it. A smaller catchment area also meant lesser travel distance and time for water to reach the gauge. Hence adjusting for a one-day lag was sufficient. SG447, on the other hand, was situated further downstream and had a great drainage area. This meant a larger travel time, which was further amplified by the routing algorithm. Hence, a two-day lag correction was found necessary at this gauge.

[47] However, there would be a threshold value beyond which the response lag time would remain constant. At that size of the catchment area, the travel time from the nearer pixels would take over the dominance from those of the farther pixels. Hence, a slightly more spread out response would be observed, with no increase in response lag. Another validation of stream discharge at a gauge further downstream could have provided some information on the threshold value for the response time lag. Such a validation was not possible due to nonavailability of data at the downstream gauges for the particular time period.

3.5. What Are the Limitations and Caveats of the Study?

[48] The method of implementing the surface runoff and seepage fluxes introduced a lag in the response time of the pixels. While it is preferable to be able to update the soil moisture states at much smaller time steps (i.e., minutes and hours), it was felt that for the reasons of computational efficiency, a daily time step was reasonable. The computation of the surface runoff and the updating of the soil moisture states of each of the pixels had to be done offline since HYDRUS-3-D does not currently have the capability to handle this. This process consumes considerable computation time. Although a high degree of correlation was observed between soil moisture signatures across scales, some of the loss of correlation may be explained by our choice of form for the scale parameter η. The η value was based on the linear distance between nodes in the FE mesh and was derived from simple topographies [*Jana and Mohanty*, 2012]. However, especially at the surface, the soil formation and deposition patterns would not be linear. With simple nonlinear configurations such as purely convex or concave slopes, the linear distance is an acceptable approximation of the actual distance and path of the water flow. When the two points i and j at which the parameters are aggregated are close to each other, approximation of the curved distance as a straight line may be considered reasonable. At large separations between i and j, this approximation is still justifiable due to fact that in this case, the support between p_i and p_j is small, and hence, minor differences in distance may be ignored. However, for more complex nonlinear topographies as encountered in this hillslope scale study, the linear distance approximation could introduce larger errors. A more comprehensive form of the scale parameter would need to be formulated based on actual travel distance between locations, especially at the surface. Also, local slope and aspect would need to be accounted for in this parameter. Based on the analysis in section 3.5, it may also be necessary to incorporate a vegetation component into the scale parameter, especially at large supports. Also, this algorithm may be incorporated into existing scaling schemes [e.g., *Zhu et al.*, 2004] which do not consider topographic variations, to make them more comprehensive.

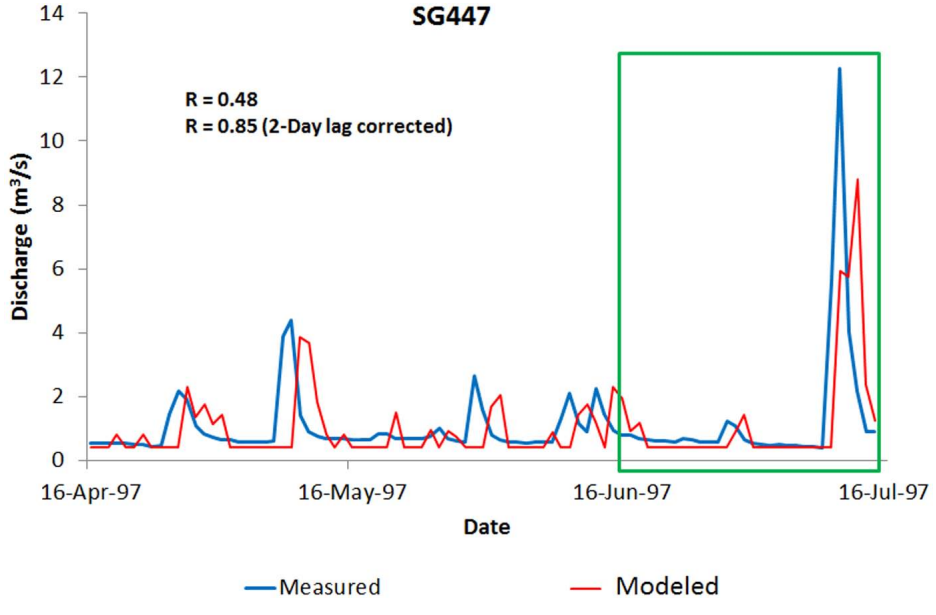

Figure 13. Stream discharge measured at downstream gauge SG447 in LW watershed.

[49] HYDRUS-3-D solves the Richard's equation, which was developed at the continuum scale and is valid for small supports. However, its validity at such large domains has recently been debated often [*Beven*, 2001; *Downer and Ogden*, 2003; *van Dam and Feddes*, 2000]. It has been shown that application of Richards' equation at large scales results in over- or underestimation of soil moisture. Since HYDRUS solves the Richards' equation for the 1000 m × 1000 m pixel domain in our study, it is reasonable to expect some deviations from the true values for the soil moisture states at the coarser pixel scales.

[50] The pixel domains in this study encompass a maximum of five soil pedons, with some having as few as two soils. In such a scenario it is not practical to apply the upscaling algorithm with only a portion of the soil information available. However, future work in this direction, when considering larger pixel domains that could potentially encompasses greater number of soils, could include studies to determine the robustness of the method when only partial information is used, i.e., by varying the sampling density. This could further lead to newer sampling schemes for soil information. Also, comparison of scaling performance of the methodology presented in this article with those of other available methods, which may or may not account for topographic variability in their upscaling algorithms would provide insight into how much the inclusion of topography could influence the outputs of the hydrologic models. Such a study is left as part of future work.

4. Conclusions

[51] We successfully upscaled soil hydraulic parameters from the 30 m resolution to a 1 km resolution at two locations—the Little Washita watershed in Oklahoma, and the Walnut Creek watershed in Iowa. Using a scale parameter, based only on the topography of the domain, in the power averaging operator algorithm, we have aggregated fine scale soil hydraulic parameters to the coarse scale for all pixels in the watershed. The equivalence of the upscaled parameters was tested by simulating water flow for the watershed pixels in HYDRUS-3-D model. An algorithm was developed and implemented around the HYDRUS-3-D framework to account for routing the surface runoff fluxes between pixels at the coarse scale.

[52] The simulated soil moisture distributions were compared across scale, and also with measurements made using the ESTAR airborne sensor during the SGP97 hydrology experiment at the LW watershed, and with PSR sensor during SMEX02 experiment in WC. Correlations of simulated and observed soil moistures were compared across time, landscape position/location, elevation, vegetative cover, and with respect to topographic indices. Inclusion of topography in the hydraulic parameter scaling algorithm, and incorporating a surface flux routing scheme, accounts for much of the variability in soil moisture across scales. While the upscaling algorithm employed did not give perfectly equivalent soil hydraulic parameters at coarser scales, reasonably good correlations between fine and coarse resolution results for simulated soil moisture states were obtained. Based on the topography, the scaling algorithm was able to capture much of the variation in soil hydraulic parameter required to generate equivalent flows and soil moisture states in a coarsened domain.

[53] Comparison of stream discharge at two gauging stations in LW also provided reasonable validation of the upscaling algorithm. A further improvement in the prediction of equivalent soil hydraulic parameters may be achieved by modifying the form of the scale parameter to include more geophysical factors and complexities. Overall, the upscaling algorithm developed based on the topography performed reasonably well in providing equivalent soil hydraulic parameter values for the Little Washita and Walnut Creek watersheds at 1 km resolutions from 30 m data.

[54] **Acknowledgments.** We acknowledge the partial support of NASA Earth System Science Fellowship (NNX06AF95H), National Science Foundation (CMG/DMS grant 062,113 and C10-00021) and NASA THPs (NNX08AF55G and NNX09AK73G) grants. We would also like to thank the editors and reviewers of this manuscript for their excellent suggestions for improvement of the article.

References

Allen, P. B., and J. W. Naney (1991), *Hydrology of Little Washita River Watershed, Oklahoma: Data and Analyses*, USDA, ARS. U. S. GPO, Washington, DC.

Beven, K. J. (2001), How far can we go in distributed hydrological modelling?, *Hydrol. Earth Sys. Sci. 5*, 1–12.

Beven, K. J., M. J. Kirkby, N. Schofield, and A. F. Tagg (1984), Testing a physically-based flood forecasting-model (Topmodel) for three UK catchments, *J. Hydrol. 69*(1), 119–143.

Bloschl, G., and M. Sivapalan (1997), Process controls on regional flood frequency: Coefficient of variation and basin scale, *Water Resour. Res. 33*(12), 2967–2980.

Das, N. N., B. P. Mohanty, and E. G. Njoku (2008), A Markov chain Monte Carlo algorithm for upscaled soil-vegetation-atmosphere-transfer modeling to evaluate satellite-based soil moisture measurements, *Water Resour. Res. 44*, W05416, doi:10.1029/2007WR006472.

Doriaswamy, P. C., J. L. Hatfield, T. J. Jackson, B. Akhmedov, J. Prueger, and A. Stern (2004), Crop condition and yield simulations using Landsat and MODIS, *Remote Sensing Environ.*, *92*, 548–559.

Downer, C. W., and F. L. Ogden (2003), Appropriate vertical discretization of Richards' equation for two-dimensional watershed-scale modelling, *Hydrol. Earth Sys. Sci. 18*, 1–22.

Elliott, R., F. Schiebe, K. Crawford, K. Peter, and W. Puckett (1993), A unique data capability for natural resources studies, paper 93-2529, presented at Int. Winter Meeting, Am. Soc. Agr. Eng., Chicago, Ill., Dec. 14–17.

Engesgaard, P., and R. Traberg (1996), Contaminant transport at a waste residue deposit: 2. Geochemical transport modeling, *Water Resour. Res. 32*(4), 939–951, doi:10.1029/95WR03822.

Famiglietti, J. S., J. W. Rudnicki, and M. Rodell (1998), Variability in surface moisture content along a hillslope transect: Rattlesnake Hill, Texas, *J. Hydrol. 210*(1–4), 259–281.

Famiglietti, J. S., D. Ryu, A. A. Berg, M. Rodell, and T. J. Jackson (2008), Field observations of soil moisture variability across scales, *Water Resour. Res. 44*, W01423, doi:10.1029/2006WR005804.

Feddes, R. A., P. J. Kowalik, and H. Zaradny (1978), *Simulation of Field Water Use and Crop Yield*, John Wiley, New York.

Hawley, M. E., T. J. Jackson, and R. H. Mccuen (1983), Surface soil-moisture variation on small agricultural watersheds, *J. Hydrol. 62*(1–4), 179–200.

Hillel, D. (1991), *Introduction to Soil Physics*, Academic, New York.

Jackson, T. J., D. M. Le Vine, A. Hsu, A. Oldak, C. T. Swift, J. D. Isham, and M. Haken (1999), Soil moisture mapping at regional scales using microwave radiometry: The Southern Great Plains Hydrology Experiment, *IEEE Trans. Geosci. Remote Sensing*, *37*(5), 2136–2151.

Jana, R. B., and B. P. Mohanty (2012), On topographic controls of soil hydraulic parameter scaling at hillslope scales, *Water Resour. Res.*, doi:10.1029/2011WR011204, in press.

Kirkby, M. J. (1975), Hydrograph modeling strategies, in *Process in Physical and Human Geography*, edited by R. Peel, M. Chisholm and P. Haggett, pp. 69–90, Heinemann, London.

Kohnke, H., and D. P. Franzmeier (1995), *Soil Science Simplified*, 4th ed., Waveland Press, Long Grove, IL.

Kustas, W. P., T. J. Jackson, J. L. Prueger, and M. C. Anderson (2003), Remote sensing field experiments for evaluating soil moisture retrieval

algorithms and modeling land-atmosphere dynamics in central Iowa, *Eos Trans., AGU*, *84*, 485–493.

Lag, J. (1951), Illustration of influence of topography on depth of a-2-layer in Podzol profiles, *Soil Sci. 71*(2), 125–127.

Miller, E. E., and R. D. Miller (1956), Physical theory for capillary flow phenomena, *J. Appl. Phys. 27*(4), 324–332.

Mohanty, B. P., and Z. Mousli (2000), Saturated hydraulic conductivity and soil water retention properties across a soil-slope transition, *Water Resour. Res.*, *36*(11), 3311–3324, doi:10.1029/2000WR900216.

Mohanty, B. P., and J. Zhu (2007), Effective averaging schemes for hydraulic parameters in horizontally and vertically heterogeneous soils, *J. Hydrometeor.*, *8*(4), 715–729.

Mohanty, B. P., P. J. Shouse, D. A. Miller, and M. T. van Genuchten (2002), Soil property database: Southern Great Plains 1997 Hydrology Experiment, *Water Resour. Res.*, *38*(5), 1047, doi:10.1029/2000WR000076.

Pradhan, N. R., Y. Tachikawa, and K. Takara (2006), A downscaling method of topographic index distribution for matching the scales of model application and parameter identification, *Hydrol. Process.*, *20*(6), 1385–1405, doi:10.1002/Hyp.6098.

Schaap, M. G., F. J. Leij, and M. T. Van Genuchten (2001), Rosetta: a computer program for estimating soil hydraulic parameters with hierarchical pedotransfer functions, *J. Hydrol. 251*(3–4), 163–176.

Schilling, K. E., and M. Helmers (2008), Effects of subsurface drainage tiles on streamflow in Iowa watersheds: Exploratory hydrograph analysis, *Hydrol. Processes*, *22*, 4497–4506.

Seibert, J., J. Stendahl, and R. Sørensen (2007), Topographical influences on soil properties in boreal forests, *Geoderma*, *141*(1–2), 139–148.

Šimůnek, J., M. T. V. Genuchten, and M. Šejna (2006), The HYDRUS software package for simulating two- and three-dimensional movement of water, heat, and multiple solutes in variably-saturated media: Technical manual, Version 1.0, edited, PC-Progress, Prague, Czech Republic.

Tarboton, D. G. (1997), A new method for the determination of flow directions and contributing areas in grid digital elevation models, *Water Resour. Res. 33*(2), 309–319.

Tedrow, J. C. F. (1951), Influence of topography and position on classification of soils having impeded drainage, *Soil Science*, *71*(6), 429–438.

van Dam, J. C., and R. A. Feddes (2000), Numerical simulation of infiltration, evaporation and shallow groundwater levels with the Richards' equation, *J. Hydrol. 233*, 72–85.

Vereecken, H., R. Kasteel, J. Vanderborght, and T. Harter (2007), Upscaling hydraulic properties and soil water flow processes in heterogeneous soils: A review, *Vadose Zone J.*, *6*, 1–28.

Western, A. W., R. B. Grayson, G. Bloschl, G. R. Willgoose, and T. A. McMahon (1999), Observed spatial organization of soil moisture and its relation to terrain indices, *Water Resour. Res.*, *35*, 797–810.

Western, A. W., S. L. Zhou, R. B. Grayson, T. A. McMahon, G. Bloschl, and D. J. Wilson (2004), Spatial correlation of soil moisture in small catchments and its relationship to dominant spatial hydrological processes, *J. Hydrol. 286*(1), 113–134. doi:10.1016/j.jhydrol.2003.09.014.

Williams, J., R. G. Barry, and W. M. Washington (1974), Simulation of the atmospheric circulation using NCAR global circulation model with ice age boundary conditions, *J. App. Meteor. 13*(3), 305–317.

Wilson, D. J., A. W. Western, and R. B. Grayson (2004), Identifying and quantifying sources of variability in temporal and spatial soil moisture observations, *Water Resour. Res. 40*(2), W02507, doi:10.1029/2003WR002306.

Wu, J., and H. Li (2006), Concepts of scale and scaling, in *Scaling and Uncertainty Analysis in Ecology: Methods and Applications*, edited by J. Wu, et al., pp. 3–15, Springer, New York.

Yager, R. R. (2001), The power average operator, *IEEE Trans. Syst. Man Cybernetics Part A Syst. Humans*, *31*(6), 724–731.

Yeh, P. J. F., and E. A. B. Eltahir (1998), Stochastic analysis of the relationship between topography and the spatial distribution of soil moisture, *Water Resour. Res. 34*(5), 1251–1263.

Zhu, J., and B. P. Mohanty (2002a), Upscaling of soil hydraulic properties for steady state evaporation and infiltration, *Water Resour. Res. 38*(9), 1178, doi:10.1029/2001WR000704.

Zhu, J., and B. P. Mohanty (2002b), Spatial averaging of van Genuchten hydraulic parameters for steady-state flow in heterogeneous soils: Aa numerical study, *Vadose Zone J.*, *1*(2), 261–272.

Zhu, J., and B. P. Mohanty (2002c), Analytical solutions for steady state vertical infiltration, *Water Resour. Res. 38*(8), 1145, doi:10.1029/2001WR000398.

Zhu, J., and B. P. Mohanty (2003), Upscaling of hydraulic properties of heterogeneous soils, in *Scaling Methods in Soil Physics*, edited by Y. A. Pachepsky, D. E. Radcliffe, and H. M. Selim, pp. 97–118, CRC Press, Boca Raton, Fla.

Zhu, J., and B. P. Mohanty (2004), Soil hydraulic parameter upscaling for steady-state flow with root water uptake, *Vadose Zone J.*, *3*, 1464–1470.

Zhu, J., and B. P. Mohanty (2006), Effective scaling factor for transient infiltration in heterogeneous soils, *J. Hydrol. 319*, 96–108.

Zhu, J., B. P. Mohanty, A. W. Warrick, and M. T. van Genuchten (2004), Correspondence and upscaling of hydraulic functions for steady-state flow in heterogeneous soils, *Vadose Zone J.*, *3*, 527–533.

Zhu, J., B. P. Mohanty, and N. N. Das (2006), On the effective averaging schemes of hydraulic properties at the landscape scale, *Vadose Zone J.*, *5*, 308–316.

R. B. Jana and B. P. Mohanty, Department of Biological and Agricultural Engineering, Texas A&M University, 142 Scoates Hall, MS 2117, College Station, TX 77843-2117, USA. (bmohanty@tamu.edu)